International Journal of Mass Spectrometry xxx (2014) xxx–xxx

Contents lists available at ScienceDirect

International Journal of Mass Spectrometry

journal homepage: www.elsevier.com/locate/ijms

An IMS–IMS threshold method for semi-quantitative determination of activation barriers: Interconversion of proline *cis* ↔ *trans* forms in triply protonated bradykinin

Nicholas A. Pierson, David E. Clemmer *

Department of Chemistry, Indiana University, Bloomington, IN 47405, United States

ARTICLE INFO

Article history:
Received 30 April 2014
Received in revised form 27 June 2014
Accepted 1 July 2014
Available online xxx

Keywords:
Ion mobility spectrometry
Multi-dimensional
Peptide conformation
Activation energy

ABSTRACT

Collisional activation of selected conformations by multidimensional ion mobility spectrometry (IMS–IMS), combined with mass spectrometry (MS), is described as a method to determine semi-quantitative activation energies for interconversion of different structures of the nonapeptide bradykinin (BK, Arg-Pro-Pro-Gly-Phe-Ser-Pro-Phe-Arg). This analysis is based on a calibration involving collision-induced dissociation measurements of ions with known dissociation energies (i.e., "thermometer" ions) such as leucine enkephalin, BK, and amino acid–metal cation systems. The energetic barriers between six conformations of $[BK + 3H]^{3+}$ range from 0.23 ± 0.01 to 0.55 ± 0.03 eV. Prior results indicate that the major peaks in the IMS distributions correspond to specific combinations of *cis* and *trans* configurations of the three proline residues in the peptide sequence. The analysis allows us to directly assess pathways for specific transitions. The combination of structural assignments, experimentally determined barrier heights, onset of the quasi-equilibrium region, and dissociation threshold are used to derive a semi-quantitative potential energy surface for main features of $[BK + 3H]^{3+}$.

1. Introduction

The biological activity of polypeptides is intrinsically tied to the structures and dynamics of the interacting species [1]. It is therefore important to consider not only the native structure, which is often assumed to be a single geometry of low energy, but also the ensemble of other structures that may exist transiently. A valuable means of understanding the multitude of possible structures and pathways associated with specific transitions is through examination of a biomolecule's energy landscape. In the past 20 years, conventional views of the "protein-folding problem" shifted from a strict pathway-dependent model involving a series of on- and off-route intermediates [2–4], to a more diffusion-driven funnel concept [5–8]. The latter idea involves a rough-surfaced landscape that consists of many local minima along a generally downhill path to the global minimum, i.e., the native structure [6]. These models help us to visualize the major structural transitions in proteins and guide computations; with a few exceptions [9,10], a detailed understanding of intermediate states (and transitions between them) is lacking – largely because of the inability of existing experimental methods to isolate and probe key intermediates, and assess barriers and pathways associated with specific transitions along the potential energy landscape.

In this paper, we analyze the nonapeptide bradykinin (BK), having the sequence Arg-Pro-Pro-Gly-Phe-Ser-Pro-Phe-Arg after it has been electrosprayed into the gas phase as $[M + 3H]^{3+}$ ions. BK is a peptide hormone, which was successfully isolated by Andrade and Silva in 1956 [11] and in 1964 was used as the first biologically relevant application of Merrifield's solid-phase peptide synthesis approach [12]. Because of its relatively small size and the fact that it was available synthetically, BK has become an important model system for structural studies in solution as well as the gas phase. In the gas phase (the emphasis of this paper), Bowers and co-workers chose BK as the first peptide to be studied by ion mobility spectrometry (IMS) techniques [13]. The mobility of an ion through a buffer gas under the influence of a weak electric field depends upon the ion's shape and charge [14–18]. Their first measurements, combined with detailed molecular modeling [19] and collision cross section calculations [20–22], showed that singly charged BK adopts a tightly-folded globular structure. In other early studies of BK in the gas phase, Williams and co-workers investigated the reactivity of a series of chemically modified and amino acid deletion and substitution sequences, and showed that this ion exists as a "salt-bridged" structure [23]. Numerous other subsequent studies [24–29] appear to be consistent with these findings.

* Corresponding author.
E-mail address: clemmer@indiana.edu (D.E. Clemmer).

http://dx.doi.org/10.1016/j.ijms.2014.07.012
1387-3806/

Recently, we extended the studies of BK in the gas phase to include structural insight into the triply charged ion. The IMS distribution for the $[BK+3H]^{3+}$ shows many peaks and thus is substantially more complicated than the single peak observed for the singly charged ion. In this paper, we use multidimensional ion mobility spectrometry–mass spectrometry (IMS–IMS–MS) measurements to obtain a semi-quantitative understanding of the potential energy surfaces associated with the multitude of stable $[BK+3H]^{3+}$ conformers. In this approach, electrosprayed $[BK+3H]^{3+}$ ions are separated in an initial drift tube, and enter a selection and activation region [30–33]. By studying the energetic thresholds necessary to convert one structure into another, we gain an understanding of the barriers and pathways between different $[BK+3H]^{3+}$ conformations.

We begin this study with a substantial amount of prior insight about the BK system. We reported evidence for at least ten independent conformer states that vary in abundance when solution compositions (aqueous and non-aqueous mixtures of varying proportion) are changed [34]. In additional studies we investigated a set of alanine-substituted BK-analogue peptides [35]. These results showed unambiguously that the major features in the $[BK+3H]^{3+}$ IMS distributions are associated with different combinations of *cis* (*C*) and *trans* (*T*) forms of the three proline residues, Pro^2, Pro^3, and Pro^7. The three most abundant $[BK+3H]^{3+}$ conformers (referred to as the A, B, and C states) were assigned as having the following *cis*/*trans* proline configurations: A as *CCC*; B as *CTT*; and, C as *TTC*.

Finally, we have previously investigated the transitions between different $[BK+3H]^{3+}$ conformations, and found that above a critical activation voltage all of the separated conformers that are produced by electrospraying BK will reach a gas-phase quasi-equilibrium (QE) distribution [36]. This is important as it allows us to distinguish between features that correspond to conformers coming from solution and those that are formed by activation in the solvent-free, gas-phase environment.

2. Experimental methods

2.1. Sample preparation

BK (≥98% purity) and leucine enkephalin (YGGFL, ≥95%) were purchased from Sigma–Aldrich (St. Louis, MO, U.S.A.), and used as received. Peptide ions were produced by positive-mode electrospray ionization (ESI) of 10^{-5} M solutions in 49:49:2 water:methanol:acetic acid. Amino acids (AAs) asparagine, aspartic acid, glutamic acid, glutamine, methionine, and proline (>99%, Fluka; Buchs, Switzerland) were dissolved in 50:50 (% volume) acetonitrile:water solutions at a concentration of $\sim 10^{-3}$ M. Sodium acetate (99.9%, Fisher Scientific; Fair Lawn, NJ, U.S.A.), potassium acetate (>99%, Aldrich; Milwaukee, WI, U.S.A.), and lithium acetate (99.99%, Sigma–Aldrich; St. Louis, MO, U.S.A.) were added to the AA solutions resulting in a concentration of $\sim 5 \times 10^{-3}$ M metal acetate.

2.2. Instrumentation

A schematic diagram of the two-meter IMS–IMS–time-of-flight MS instrument used in these studies is shown in Fig. 1. IMS theory [20,22,37,38] and applications [39–46] are described in detail previously. A brief description of the experiment is as follows: ions were produced by a chip-based ESI autosampler (Advion Biosciences, Inc., Ithaca, NY, U.S.A.) and trapped in an ion funnel [47,48] labeled F1 in Fig. 1. A 150 μs-wide pulse applied to G1 was used to gate a packet of ions into the drift tube. Driven by a $10\,V \times cm^{-1}$ electric field, the ions were separated on the basis of their low-field mobilities through 3.00 ± 0.01 Torr He. Upon exiting the drift tube, ions were focused through a differential pumping region and pulsed orthogonally into a two-stage reflectron-geometry time-of-flight mass spectrometer for nested drift time (m/z) measurement [49].

2.3. Multidimensional IMS

The drift tube illustrated in Fig. 1 is divided into two effective drift regions (D1 and D2) by ion funnel F2, which also contains 3.00 ± 0.01 Torr He buffer gas. One purpose of funnels F2 and F3 is to refocus radially diffuse ions toward the center axis to avoid ion loss through the instrument; this is accomplished through the use of an rf-focusing component, as well as operating at a slightly higher ($12\,V \times cm^{-1}$) linear electric field. F2 also contains non-rf ion selection (G2) and ion activation (IA2) regions utilized in these multidimensional IMS experiments. A delay pulse lowers a repulsive potential across G2 for 30–100 μs, thus allowing ions with a narrow range of mobilities to pass; all other ions reach an electrostatic-potential barrier and are neutralized. Timing of the delay pulse is adjusted with respect to the initial source pulse from G1 in order to isolate ions of a desired mobility from the total distribution. A new population of ions can be formed from the selected ions prior to entering D2 by application of a voltage drop across the 0.3-cm activation region (IA2); for these experiments, the ion activation voltage (V) was varied between 0 V and 260 V ($\sim$0–$870\,V \times cm^{-1}$ above the drift field) to collisionally activate

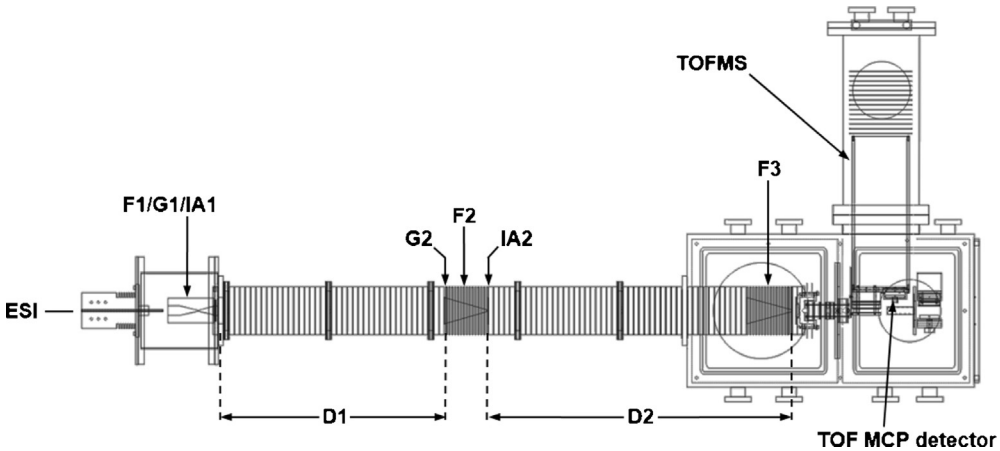

Fig. 1. Schematic diagram of the ~2-m IMS–IMS–MS instrument employed in these studies; the mid-drift tube ion funnel F2 includes mobility selection gate G2 and the 0.3-cm IA2 activation region where the electric field can be varied to tune the energy of ion–molecule collisions.

Please cite this article in press as: N.A. Pierson, D.E. Clemmer, An IMS–IMS threshold method for semi-quantitative determination of activation barriers: Interconversion of proline *cis*↔*trans* forms in triply protonated bradykinin, Int. J. Mass Spectrom. (2014), http://dx.doi.org/10.1016/j.ijms.2014.07.012

selected ions via ion–neutral collisions with the He buffer gas. Approximately 10^3–10^4 collisions are estimated to occur in this 0.3-cm region. Conformational transitions can be induced with moderate electric fields (e.g., 50–200 V × cm^{-1} for $[BK+3H]^{3+}$), whereas collision-induced dissociation (CID) can occur at higher IA2 fields (e.g., 240–530 V × cm^{-1} for $[BK+3H]^{3+}$). Upon exiting the high-field IA2 region, ions are thermalized to room temperature (298 K) and drift through D2.

2.4. Collision cross section measurements

Collision cross sections (Ω) of ions were determined from drift times (t_D) according to the following relationship [14]:

$$\Omega = \frac{(18\pi)^{1/2}}{16}\frac{ze}{(k_B T)^{1/2}}\left[\frac{1}{m_I}+\frac{1}{m_B}\right]^{1/2}\frac{t_D E 760}{L}\frac{T}{P}\frac{1}{273.2N},$$

where k_B is the Boltzmann constant, T is temperature (298 K for these studies), m_I and z are the mass and charge of the ion, respectively, m_B is the mass of the buffer gas, E is the electric field, L is the length of the drift tube, P is the pressure, and N is the neutral number density of the buffer gas at standard temperature and pressure.

2.5. Molecular modeling

Molecular dynamics simulations were carried out on $[BK+3H]^{3+}$ with the extensible and systematic force field (ESFF) in the Discover3/InsightII software suite (Accelrys, Inc., San Diego, CA, U.S.A.). The guanidine groups of Arg^1 and Arg^9 side-chains were protonated, as well as the amino terminus [35]. Random-coil geometries were obtained from energy minimized structures before initiating dynamics steps that would allow the ion to fold and establish energetically favorable intramolecular interactions; initial, extended structures of BK were randomized, followed by 1000 cycles of steepest descent (1 kcal/mol × Å tolerance) and conjugate gradient (0.01 kcal/mol × Å tolerance) energy minimization; the resulting structures were saved. Representative low-energy BK trial geometries were obtained through dynamics simulations performed at 298 K in vacuo (dielectric constant, $\varepsilon = 1$) for 20 ns (1 fs step); structures were energy minimized (as described above) and saved every 100 ps; each energy-minimized structure served as the input for the subsequent round of dynamics. Trajectory method collision cross section values were calculated using MOBCAL [22,50].

3. Results and discussion

Fig. 2 shows the IMS distribution for $[BK+3H]^{3+}$ on a collision cross section scale. Six conformations, labeled A–F, were selected and activated by IMS–IMS, as described in detail previously [36]. Integrated peak areas for $[BK+3H]^{3+}$ conformers and fragmentation products are shown as a function of IA2 activation voltage in Fig. 3. In general, the selected conformation undergoes collision-induced conformational transitions over a wide range of moderate activation voltages from ~15 V to 75 V. This can be observed by visual inspection of the plots which show depletion of each initially selected conformer. Normalized abundances of A–C become relatively constant between ~52 and ~75 V; above this activation voltage, CID of the $[BK+3H]^{3+}$ ions is observed. The relative abundances of A (~2%), B (16%), and C (80%) across this intermediate range of activation voltages is reproducible for all selections A–F, and thus signifies the formation of the QE distribution, which we have described in detail previously [36]. Below, we focus on the thresholds for conformational transitions in each of these six IMS–IMS–MS data sets.

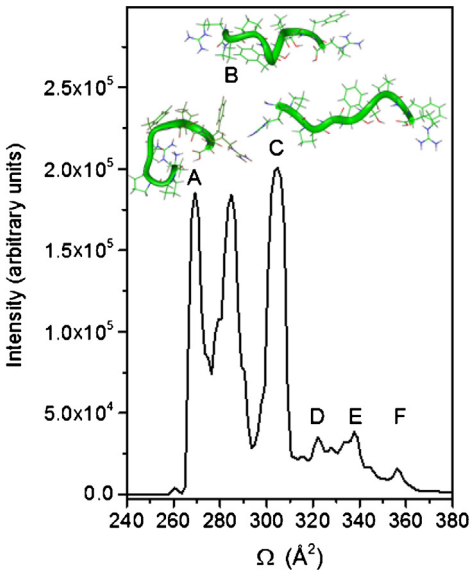

Fig. 2. IMS distribution of $[BK+3H]^{3+}$ plotted on a collision cross section scale. Conformations A–F are labeled as previously assigned [36]. Low-energy trial geometries for A–C in agreement with experimental collision cross section values (within 2%) and *cis*/*trans* proline assignments detailed in-text.

3.1. Threshold analysis

We begin by noting that we have used an arbitrary definition of a change in relative intensity of 1% as an indication for a threshold event; in these data, this value represents a point at which the signal-to-noise ratio is sufficient to confidently detect the formation of a new ion population. This approach is similar to one used by Cassady et al. [51], and is not based on statistical theories as are more rigorous methods for threshold analysis developed by Armentrout and co-workers [52,53]. We note that in most cases the barriers for interconversions reported here are self-consistent for the six BK conformations we studied; however, limitations of this method are discussed below.

The region associated with the threshold for activation for $[BK+3H]^{3+}$ transitions is expanded to the right of each plot in Fig. 3. From this figure we see that some of the transitions are easily distinguished, requiring very different voltages at threshold to induce a transition. For example, the formation of B and C from selection and activation of conformation A are separated by 8 V (18 and 26 V, respectively). Similarly, the thresholds to form A and B from activation of conformer C are very different (~36 and 27 V, respectively). These data indicate measurable differences in the energy barrier heights between specific state-to-state transitions. Thresholds for $[BK+3H]^{3+}$ conformers A (23 V) and C (24 V) formed from activation of B, however, are very similar; these data suggest very similar barrier heights for these particular transition events. It is important to note that activation of elongated conformers D, E and F only produce conformers A–C, and transitions between the elongated conformers were not observed. Conversely, the activation barriers can be measured in both forward and reverse directions for interconversions that involve only conformers A–C. This point is discussed in more detail below. The threshold data presented in Fig. 3 and the relative differences between all of the various transitions are somewhat interesting in a qualitative sense; however, expression of these activation magnitudes as energies (instead of instrument-specific voltages) is more broadly relevant towards understanding peptide structure and conformation-specific thermochemical information.

Please cite this article in press as: N.A. Pierson, D.E. Clemmer, An IMS–IMS threshold method for semi-quantitative determination of activation barriers: Interconversion of proline *cis*↔*trans* forms in triply protonated bradykinin, Int. J. Mass Spectrom. (2014), http://dx.doi.org/10.1016/j.ijms.2014.07.012

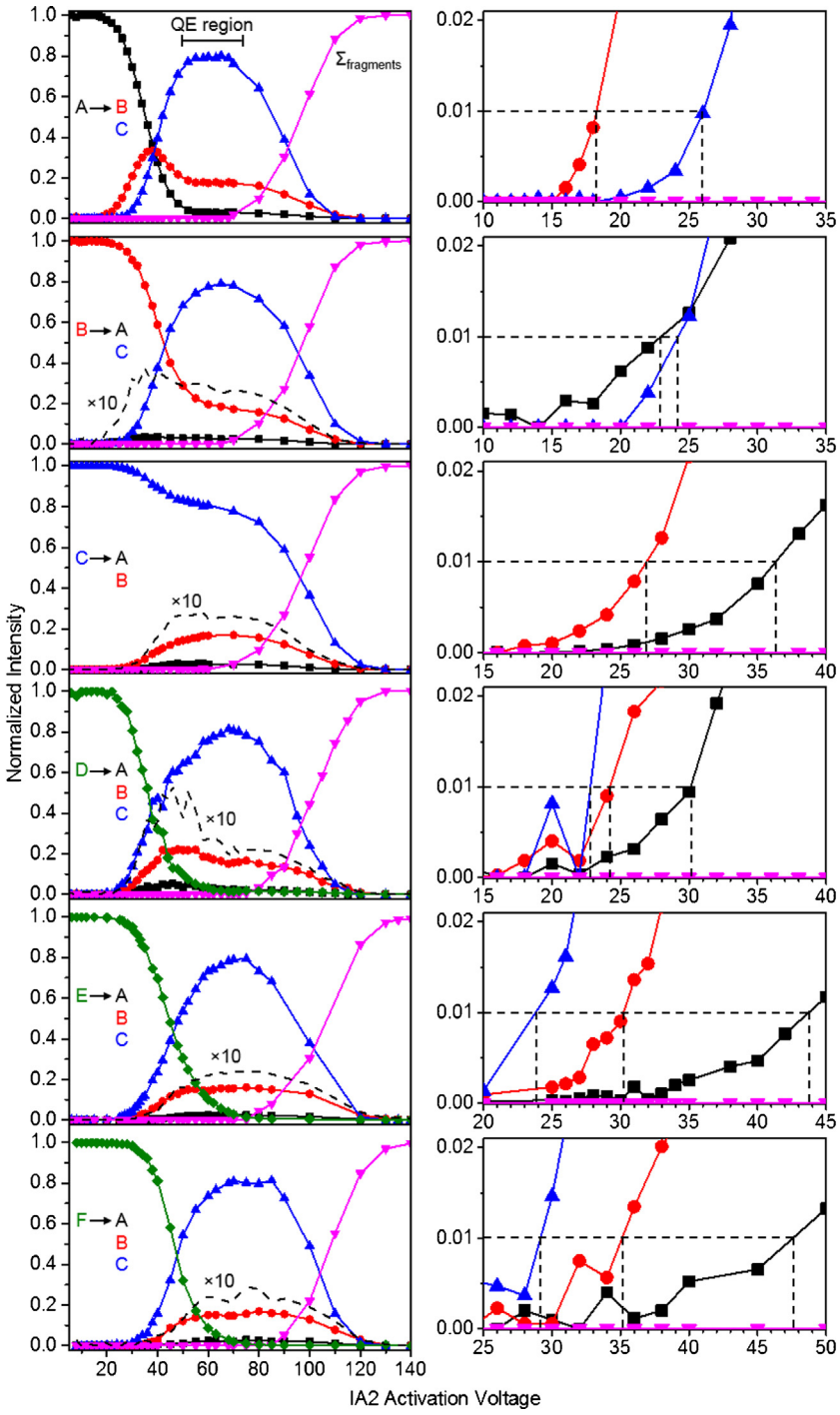

Fig. 3. Normalized peak integrations for six $[BK+3H]^{3+}$ conformers A–F from IMS–IMS selection and voltage-resolved activation experiments. The quasi-equilibrium (QE) region is defined as the range of activation voltages that result in the formation of relatively constant abundances of conformers A–C prior to fragmentation. Each plot is expanded on the right to show the threshold transition regions for each experiment; dashed lines indicate the 1% relative abundance criteria for threshold analysis.

3.2. Development of an IMS–IMS activation energy (E_a) scale

In order to convert the IA2 excitation voltage measurements into energies, we have developed a relatively simple calibration. This calibration is based on IMS–IMS measurements of CID thresholds of well-characterized systems, using conditions that are similar to those used for the QE study [36]. These systems include CID of BK, $[AA+Cat]^+$ complexes (where Cat represents a Group I metal cation), and protonated YGGFL. McLuckey and co-workers measured the E_a for dissociation of $[BK+3H]^{3+}$ to its lowest-energy fragment $[BK-H_2O+3H]^{3+}$ to be 0.79 ± 0.03 eV from thermal dissociation experiments in a quadrupole ion trap [54]. Direct comparison of the IA2 activation voltage required for $[BK+3H]^{3+}$ dissociation to the published E_a value, along with other previously reported systems detailed below, provides a calibration to determine threshold activation energies for gas-phase transitions of the six $[BK+3H]^{3+}$ conformations. Replicate IMS–IMS experiments yielded an average IA2 voltage of 73 ± 7 V for

Please cite this article in press as: N.A. Pierson, D.E. Clemmer, An IMS–IMS threshold method for semi-quantitative determination of activation barriers: Interconversion of proline *cis*↔*trans* forms in triply protonated bradykinin, Int. J. Mass Spectrom. (2014), http://dx.doi.org/10.1016/j.ijms.2014.07.012

$[BK+3H]^{3+}$ fragmentation. We address conformer-specific fragmentation thresholds in detail below in the context of activation energies and relative potential well depths.

CID analysis of cationized AAs provides a starting point for the IMS–IMS energy calibration because the single-collision conditions employed in guided ion beam MS studies can yield accurate and precise E_a values [52,53,55,56]; moreover, the relatively small size of these systems makes them amenable to high-level theoretical calculations (e.g., ab initio and density functional theories) that are often used to corroborate the experimental measurements of bond dissociation energies. Monomer ions of ten cationized AAs were selected by IMS–IMS, and voltage-resolved activation was performed up to voltages that achieved 100% precursor ion dissociation (data not shown). CID thresholds were determined by the onset of selected precursor ion fragmentation according to the 1% criteria described above. With the exception of the lithiated AAs, the fragmentation threshold was indicated by the appearance of the lone metal cation. For $[Pro+Li]^+$ and $[Met+Li]^+$, however, internal fragmentation resulting in neutral losses were observed at the fragmentation threshold, as reported previously [57,58].

Table 1 lists the ten cationized AA systems used for this part of the study and their respective dissociation thresholds [57–59]. In addition to increasing the number of measurements for the voltage-to-energy calibration, the $[AA+Cat]^+$ data fill out the range of IA2 voltages similar to those that bring about conformational changes in peptides. Although IMS–CID–IMS–MS applied to small, well-characterized systems appears promising as a means of calibration, we were concerned about extrapolation of these energetic values to systems of higher complexity. Therefore, to bridge the gap of the small calibrated systems to the larger BK ion, we also carried out IMS–CID–IMS–MS selection and activation studies of another well-characterized "thermometer" ion, protonated YGGFL. The thermochemistry of $[YGGFL+H]^+$ has been examined by numerous MS techniques, leading to it being termed "a mass spectrometry standard" [60]. The lowest-energy fragmentation pathway for protonated YGGFL is the b_4 ion. As an example of the CID threshold analysis, the relative abundance of b_4 as a function of IA2 activation voltage is shown in Fig. 4. A value of 1.21 ± 0.25 eV was used as the E_a for dissociation of $[YGGFL+H]^+$ to b_4, which is the average of nine independent measurements from various ion activation techniques [60]. Although YGGFL is considered a well-characterized system, the wide range of published E_a values (0.945–1.66 eV) demonstrates that ion

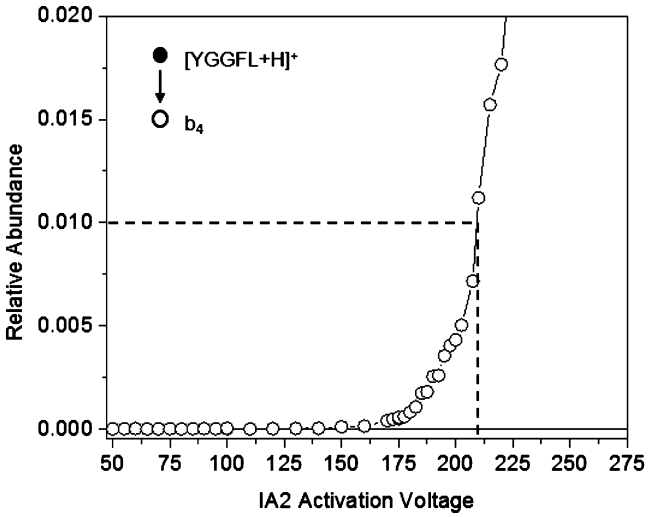

Fig. 4. Threshold CID analysis for protonated YGGFL yields formation of the b_4 ion, the lowest-energy fragmentation channel in this system.

Table 1
E_a values reported in the literature and IMS–CID–IMS–MS thresholds of cationized AAs and peptide systems measured in this study.

Ion	Degrees of freedom	E_a, eV	IA2 $V \times z$
$[Pro+K]^+$	48	1.49 (±0.05)[a]	47 (±2.4)
$[Met+K]^+$	57	1.47 (±0.11)[b]	48 (±2.4)
$[Asp+Na]^+$	45	2.02 (±0.06)[c]	63 (±3.2)
$[Asn+Na]^+$	48	2.17 (±0.06)[c]	64 (±3.2)
$[Glu+Na]^+$	54	2.06 (±0.05)[c]	63 (±3.2)
$[Gln+Na]^+$	57	2.21 (±0.06)[c]	71 (±3.6)
$[Pro+Na]^+$	48	1.93 (±0.05)[a]	59 (±3.0)
$[Met+Na]^+$	57	2.09 (±0.11)[b]	68 (±3.4)
$[Pro+Li]^+$	48	2.89 (±0.10)[a]	98 (±4.9)
$[Met+Li]^+$	57	3.33 (±0.13)[b]	108 (±5.4)
$[YGGFL+H]^+$	228	1.21 (±0.25)[d]	209 (±10.5)
$[BK+3H]^{3+}$	450	0.79 (±0.03)[e]	219 (±20)[f]

[a] 0 K bond dissociation energy value from GIBMS Ref. [57].
[b] 0 K bond dissociation energy value from GIBMS Ref. [58].
[c] 0 K bond dissociation energy value from GIBMS Ref. [59].
[d] Average value from various ion activation methods, Ref. [60].
[e] Value from thermal dissociation in a quadrupole ion trap, Ref. [54].
[f] Average value from replicate IMS–IMS experiments.

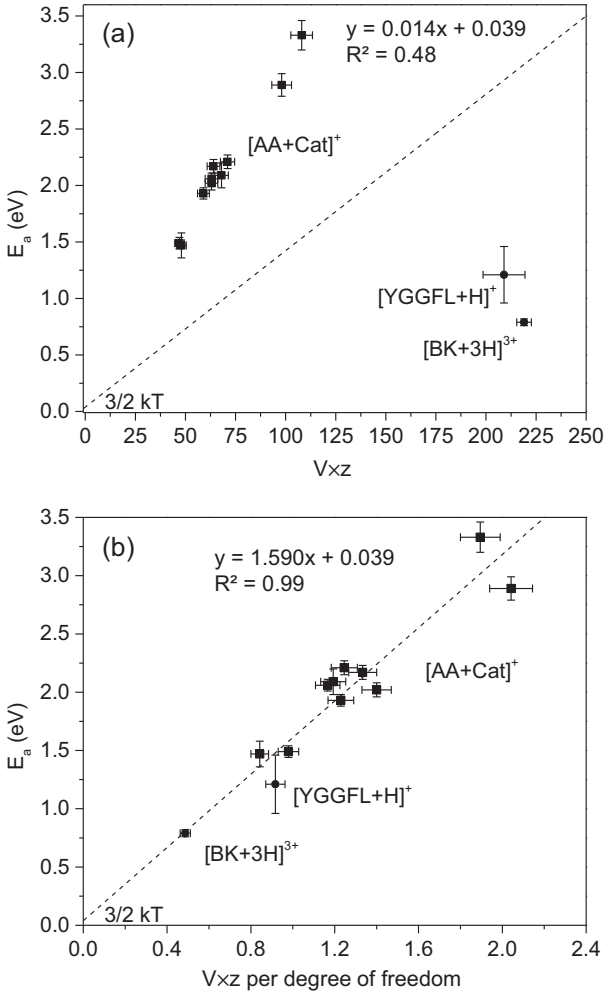

Fig. 5. Failed correlation between published E_a and IA2 $V \times z$ (a). Energy scale calibration: published E_a as a function of experimental IA2 voltage thresholds with normalization to the number of degrees of freedom ($V \times z$ per degree of freedom) for dissociation of BK, YGGFL, and amino acid–cation systems listed in Table 1 (b).

Please cite this article in press as: N.A. Pierson, D.E. Clemmer, An IMS–IMS threshold method for semi-quantitative determination of activation barriers: Interconversion of proline *cis*↔*trans* forms in triply protonated bradykinin, Int. J. Mass Spectrom. (2014), http://dx.doi.org/10.1016/j.ijms.2014.07.012

activation studies are altogether not as straightforward as the term "model system" might suggest.

Fig. 5a shows the published E_a values plotted versus CID voltage thresholds (multiplied by ion charge) from IMS–IMS–MS. It is clear to see from the plot that there is extremely poor correlation between the measurements and the literature data, suggesting that some important factor is missing. To relate all of the systems for the energy calibration, the number of vibrational degrees of freedom must also be taken into account [61,62]. Collisional activation is considered an ergodic, or slow-heating, process which results in statistical distribution of energy into all of the internal modes of the ion [63,64]. Adjusting our calibration for degrees of freedom is a crude normalization for two effects; both the average internal energy of a thermalized ion and the average lifetime of an activated ion are proportional to the number of degrees of freedom [65–67]. Examples from recent MS studies support this idea by systematically demonstrating degrees of freedom are linearly correlated to characteristic CID energies of peptides and linear polymers [68,69]. Fig. 5b represents a calibration curve in which published E_a values are plotted versus IA2 thresholds for dissociation of BK, YGGFL, and ten cationized AAs (in units of threshold voltage × charge, per degree of freedom). A weighted linear regression fit [70] to these data points was calculated with the *y*-intercept set to the kinetic energy of an ion at room temperature (3/2 k*T*, i.e., 0.039 eV), which represents the energy of ions under non-activating conditions in the 298 K drift tube. This revised calibration curve (slope = 1.590 ± 0.030), which incorporates the number of degrees of freedom in each system, shows a strong linear relationship.

3.3. Energies of conformational transitions

The revised calibration curve derived above was used to determine energetic barriers for each experimentally observed structural transition between $[BK+3H]^{3+}$ conformers. The E_a values are reported in Table 2 along with their associated uncertainties determined through propagation of error in the IA2 voltage measurements and the uncertainty in the slope of the weighted linear regression. As mentioned above, the transitions between the A–C structures allow us to examine the activation barrier from different directions. One caveat with this method is that it cannot directly take into account entropy [63,64,71–75]. That is, the current interpretation assumes that the transition states are similar in terms of entropy of activation; i.e., the forward and reverse structural transitions are either both loose, or both tight. This seems to be the case for many of the transitions examined in this system, however, possible evidence for entropic effects are discussed below.

Table 2
IA2 voltage measurements and calculated activation energies between transitions of six $[BK+3H]^{3+}$ conformations.

$[BK+3H]^{3+}$ Conformation			
Selected	Formed	IA2 voltage	Threshold E_a, eV
A	B	18 (±0.9)	0.23 (±0.01)
	C	26 (±1.3)	0.31 (±0.02)
B	A	23 (±1.2)	0.28 (±0.02)
	C	24 (±1.2)	0.29 (±0.02)
C	A	36 (±1.8)	0.42 (±0.02)
	B	27 (±1.4)	0.33 (±0.02)
D	A	30 (±1.5)	0.36 (±0.02)
	B	24 (±1.2)	0.29 (±0.02)
	C	23 (±1.2)	0.28 (±0.02)
E	A	44 (±2.2)	0.51 (±0.03)
	B	30 (±1.5)	0.36 (±0.02)
	C	24 (±1.2)	0.29 (±0.02)
F	A	48 (±2.4)	0.55 (±0.03)
	B	35 (±1.8)	0.41 (±0.02)
	C	29 (±1.5)	0.35 (±0.02)
A	$[BK-H_2O+3H]^{3+}$	68 (±7)	0.76 (±0.08)
B	$[BK-H_2O+3H]^{3+}$	67 (±7)	0.75 (±0.08)
C	$[BK-H_2O+3H]^{3+}$	66 (±7)	0.74 (±0.08)
D	$[BK-H_2O+3H]^{3+}$	76 (±7)	0.84 (±0.09)
E	$[BK-H_2O+3H]^{3+}$	76 (±7)	0.84 (±0.09)
F	$[BK-H_2O+3H]^{3+}$	86 (±7)	0.95 (±0.10)

The thresholds for converting A to B and B to A were found to be measurably different, 0.23 ± 0.01 and 0.28 ± 0.02 eV, respectively. Therefore, the potential well for B must be placed lower relative to that of A by 0.05 ± 0.03 eV. For the transition from conformer B to C we determine $E_a = 0.29 \pm 0.02$ eV and from conformer C to B we obtain a value of $E_a = 0.33 \pm 0.02$ eV. These values indicate that the potential energy well for C lies slightly below the well for B by 0.04 ± 0.03 eV. And finally, the transition from conformers A to C occurs at $E_a = 0.31 \pm 0.02$ eV, and a value of $E_a = 0.42 \pm 0.02$ eV in the reverse direction for transition from conformer C to A. This latter result indicates that conformer C is more stable than A (consistent also with the relative intensities of the three peaks under QE conditions). Furthermore, the difference between A and C (0.11 ± 0.03 eV) is equal within error to the sum of A/B and B/C difference values (0.09 ± 0.04 eV), as expected.

Energetic barriers associated with the D–F conformers to other structures could only be determined for specific transitions. This is because the D–F states cannot be produced from any other conformer, at any activation energy used in these studies. Presumably these states require solvent to be formed, and are only produced directly from ESI of specific solutions [34,76]. Overall, we find that higher energies are required to convert elongated conformations D–F to the A–C states. For instance, the threshold energy for the formation of conformer A from selected conformer F is 0.55 ± 0.03 eV. Although these high E_a values might suggest higher entropies of activation or very deep potential wells, the relative well depths cannot be assigned without information about formation of the elongated conformations from other selected states.

3.4. Semi-quantitative potential energy surfaces for conformations of $[BK+3H]^{3+}$

It is instructive to use the barrier heights and relative well depths to generate a potential energy surface for this system. Fig. 6 shows a semi-quantitative potential energy diagram for the different conformers of $[BK+3H]^{3+}$, constructed from data described above. Minima along the surface signify low-energy conformations of $[BK+3H]^{3+}$ resolved by IMS. When all of the measured E_a values for transitions between conformers A–C are taken into account, the barriers between the states are most consistent with the wells for A–C placed relative to one another at 0.09 ± 0.02, 0.04 ± 0.02, and 0.00 ± 0.02 eV, respectively. With these potential wells fixed, the magnitudes of the barrier heights can be considered by adding each threshold E_a to its corresponding relative potential well value. Thus, the energy barrier between A and B states was determined to be 0.32 ± 0.04 eV, which is equal within error to the 0.33 ± 0.04 eV barrier between B and C. Although these two barrier heights are very close in magnitude, replicate experiments for IMS–IMS activation of B always resulted in the formation of A before C.

Based on the barriers between states A and B, and B and C, one expects that the barrier for formation of A directly from C should be limited by the highest barrier, i.e., the barrier between states B and C, which is 0.33 ± 0.02 eV higher than the lowest energy C

Please cite this article in press as: N.A. Pierson, D.E. Clemmer, An IMS–IMS threshold method for semi-quantitative determination of activation barriers: Interconversion of proline *cis*↔*trans* forms in triply protonated bradykinin, Int. J. Mass Spectrom. (2014), http://dx.doi.org/10.1016/j.ijms.2014.07.012

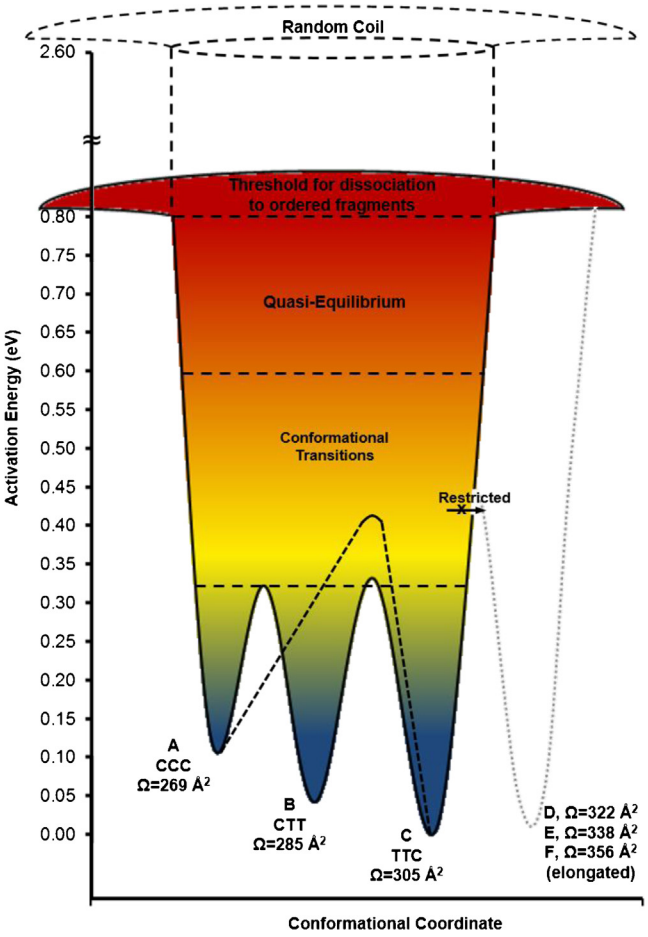

Fig. 6. Semi-quantitative conformational landscape of $[BK+3H]^{3+}$ derived from experimental barrier heights, thresholds for structural transitions, and QE region threshold, and simulated random-coil structures. The *cis*/*trans* (*C*/*T*) configurations of Pro^2, Pro^3, and Pro^7 are listed for conformers A–C, as previously assigned [35].

structure. However, in numerous measurements we find that the energy required to form A directly from C is somewhat higher, leading us to a barrier for this transition of 0.42 ± 0.02 eV. Similarly we find that formation of state C from A also occurs at a higher energy 0.31 ± 0.02 above the minimum energy for A. This indicates that the A ↔ C interconversion occurs along a different pathway. That is, there are two distinct routes between these conformers: one that involves the intermediate conformer B; and another direct route that requires ~0.1 eV more energy. While alternate pathways provide one possible explanation, another possibility is that this difference in energies is due to entropic effects.

With the barriers between conformers A–C in place, it is interesting to consider what is expected at higher degrees of activation. At intermediate energies (between 0.42 ± 0.02 and 0.59 ± 0.03 eV), activation will result in changes in conformation; but the QE distribution will not be established. Above 0.59 ± 0.03 eV, activation of any precursor leads to the formation of constant ratios of A (~2%), B (16%), and C (80%), which we have previously called the QE region prior to precursor dissociation [36]. Using these QE values as the equilibrium constant, *K*, in the expression for standard Gibbs free energy (ΔG°) yields values of 0.103 ± 0.004, 0.047 ± 0.005, and 0.006 ± 0.001 eV for A–C, respectively, in excellent agreement with each respective potential well depth determined by threshold IMS–IMS measurements.

Thus far, our potential energy diagram is based on transitions that are observed for structures that can be produced in the gas phase. Fig. 6 also illustrates how structures D–F, which appear to require solution, fit into this scheme. The barriers for states D–F (determined from the thresholds shown in Fig. 3) show that these transitions occur at higher energies than those associated with BK ion conformations that are observed to interconvert in the gas phase. This suggests the elongated D–F states might need to overcome an entropic penalty in order to form the gas-phase preferred A–C conformers. It suggests the elongated conformers were formed through solvent–molecule interactions, and are trapped during the ESI process [34,76,77], are actually lower in energy than the A–C gas-phase structures. In this case it appears that solvent helps to guide peptide ions to these configurations, and that once the solvent is eliminated, these structures remain low in energy. We are still investigating why these transitions appear to be restricted, in that conversions of A–C to any of the elongated conformations are "forbidden" in a solvent-free environment.

Precursor ion fragmentation occurs at energies beyond 0.80 ± 0.09 eV. One final set of data we include in Table 2 are the fragmentation thresholds of each individual conformer. We expected A to dissociate first, followed by B, then C with values of 0.70 ± 0.04, 0.75 ± 0.04, and 0.79 ± 0.04 eV, respectively, on the basis of the relative well depths and the threshold dissociation value of 0.79 ± 0.03 eV from McLuckey and co-workers [54]. The values, however, are opposite in relative ordering with A being 0.85 ± 0.08 eV (0.76 ± 0.08 eV E_a plus the initial well depth of 0.09 ± 0.02 eV), B being 0.79 ± 0.08 eV, and C being 0.74 ± 0.08. With the exception of A, these values are within the combined errors in expected and measured values. Nevertheless, this indicates our ability to measure IMS–IMS activation thresholds at higher energies is limited. It is worth noting that we have gone on to test the relative well depth ordering of BK A–C through parallel CID experiments [43] where, in a single IMS–MS/MS experiment, all three conformers are activated at the exit of the drift tube, thus affording direct comparison of CID thresholds; in this case, the relative thresholds agree with the well depths we have derived from barrier heights.

A final feature of this surface is associated with the loss of structure at higher energies with respect to the onset of fragmentation. One interesting finding involves the energies that we calculate for simulated random-coil structures of BK (relative to the low-energy trial geometries shown in Fig. 2). These calculations suggest that a random coil lies substantially higher in energy than do the products of fragmentation, thus indicating that fragmentation product ions must have relatively stable, defined geometries. That is, the fragment ions either retain some elements of structure from the precursor, or they rearrange to form stable products during the dissociation process. This is in agreement with the extensive body of work surrounding formation of oxazolone and diketopiperazine structures in peptide ion fragmentation [78–83].

3.5. *Conformational transitions rationalized in terms of* cis/trans *assignments*

In prior work, we used an IMS–MS analysis of alanine-substituted analogues of BK to assign the dihedral configurations of Xxx–Pro^2, Pro^3, and Pro^7 peptide bonds in conformers A–C as *CCC*, *CTT*, and *TTC*, respectively [35], as labeled in Fig. 6. The energetic analysis presented above provides additional insight about how transitions between structures occur. Scheme 1 lists all eight possible *cis*- and *trans*-Pro combinations and A–C assignments. We begin by noting that all of the *cis*/*trans* assignments that we find for peaks A–C differ by two proline *cis*/*trans* forms. That is, the A conformer (*CCC*) would need to convert two prolines (at the peptide bond dihedral angle preceding residues 3 and 7) to a *trans* configuration in order to form conformer B. Likewise, two

Please cite this article in press as: N.A. Pierson, D.E. Clemmer, An IMS–IMS threshold method for semi-quantitative determination of activation barriers: Interconversion of proline *cis* ↔ *trans* forms in triply protonated bradykinin, Int. J. Mass Spectrom. (2014), http://dx.doi.org/10.1016/j.ijms.2014.07.012

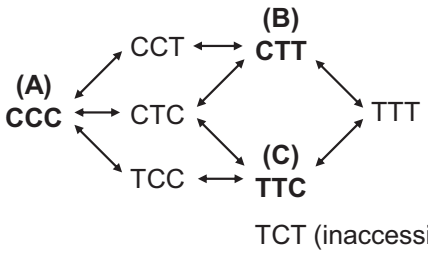

Scheme 1. Pathways for structural transitions between $[BK+3H]^{3+}$ conformers A–C rationalized through *cis*/*trans* (*C*/*T*) isomerizations of Pro^2, Pro^3, and Pro^7, as previously assigned [35].

transitions (involving residues 2 and 3) are required to form conformer C. In the absence of entropic effects, a purely enthalpic analysis of BK transitions is consistent with the connectivity between *cis*/*trans* forms shown in Scheme 1. We hypothesize that these isomeric changes must occur one at a time, and that we are simply not sensitive to this in the present analysis. Thus, we suggest that the four *cis*/*trans* combinations *CCT*, *CTC*, *TCC*, and *TTT* represent relatively unstable structures that might be intermediates between conformations A–C; this argument rests on the fact that these structures are not experimentally observed (on the basis of comparative collision cross sections of the analogs with the native BK distribution in our previous analogue peptide study). Lastly, because it would require multiple *cis*/*trans* isomerizations to reach any of the assigned A–C structures, TCT represents an inaccessible, or at least highly disfavored, intermediate for $[BK+3H]^{3+}$ conformational transitions. This is also consistent with previous results that show the lack of any $[BK+3H]^{3+}$ conformer matching the cross section for the TCT-like analogue peptide (Pro^2, Ala^7 BK) [35].

3.6. Comparison of gas- and solution-phase energetics for cis ↔ trans proline isomerization

While no direct measures of the barriers for *cis* ↔ *trans* isomerization of BK in solution exist, it is interesting to compare the magnitude of the barriers associated with transitions for $[BK+3H]^{3+}$ with *cis* ↔ *trans* transitions that have been measured in solution. Theoretical and nuclear magnetic resonance-derived barriers for *cis* ↔ *trans* isomerization of proline-containing dipeptides and smaller, amide-based molecular constructs in solution are reported to be in the range of 0.43–0.87 eV [84–88]—significantly greater than the 0.23 ± 0.01–0.42 ± 0.02 eV values that we have determined for the solvent-free A–C $[BK+3H]^{3+}$ ion interconversions. We speculate that several factors may explain the substantially larger barriers associated with the solution transitions. First, we expect that relative to solution, gas-phase $[BK+3H]^{3+}$ is destabilized by stronger repulsive Coulombic interactions arising from the low-dielectric vacuum environment. This may lower *cis* ↔ *trans* barriers in the gas phase. Additionally, we note that although the *cis* ↔ *trans* conversion is associated with rotation of only a single dihedral angle in the molecule, the motion results in a large change in the overall geometry of the peptide, as illustrated in the structures shown in Fig. 2. This case involves the need to move remaining portions of the peptide through the solvent; thus, the proline *cis* ↔ *trans* isomerization may encounter a large resistance for this transition, thereby increasing the magnitude of the barrier in solution compared with the gas phase. Certainly it will be important to measure the *cis* ↔ *trans* proline barriers for BK in solution directly in order to understand the differences associated with these transitions that arise from solvation effects.

4. Conclusions

IMS–IMS–MS studies of $[BK+3H]^{3+}$ illustrate the dynamic conformational changes that a peptide can exhibit in the collisional activation regime prior to dissociation. We presented an analysis that measures barriers in a complex, multi-conformation system for the first time. This involves the derivation of a calibrated IMS–IMS activation energy scale and its application to determine E_a values and relative barriers between six $[BK+3H]^{3+}$ conformations, which were found to occur in the range of 0.23 ± 0.01–0.55 ± 0.03 eV. These values provide an initial insight, and this approach should be used with the aforementioned limitations involving the inability to delineate entropy effects from enthalpies of activation in mind. Refinement of this method will be achieved through further activation-dependent IMS–IMS–MS studies, which are most directly applicable in the examination of conformational energetics for polypeptides of an intermediate size regime (i.e., tryptic peptides and small proteins). The present work also demonstrates that comprehensive analysis by multidimensional IMS can be used to construct a semi-quantitative gas-phase potential energy landscape of a peptide ion by combining information about barrier heights, relative well depths, conformer abundances in the QE distribution, and dissociation channels. For $[BK+3H]^{3+}$, the energy surface indicates conformer C is the lowest-energy gas-phase state, followed by B, then A. This is in agreement with the observation that C is the most abundant conformation in the gas-phase QE distribution. Consideration of *cis*/*trans* Pro isomerizations in the context of the energy surface presented here provides insight into the possible *cis*/*trans* Pro configurations of intermediates between stable BK conformations.

Acknowledgements

The authors thank Professor David Russell and Dr. Liuxi Chen at Texas A&M University for invaluable discussions involving the interpretation of BK analog results. We extend our gratitude to Professor Peter Armentrout at the University of Utah for providing critical insight of this work, and also to Dr. Brian Bohrer for helpful thoughts and feedback. These studies are supported by funding for instrumentation development from the NIH (RC1GM090797-02) and from the Indiana University METAcyte Initiative through a grant from the Lilly Endowment.

References

[1] K. Henzler-Wildman, D. Kern, Nature 450 (2007) 964–972.
[2] C. Levinthal, J. Chim. Physique 65 (1968) 44–45.
[3] A. Ikai, C. Tanford, Nature 230 (1971) 100–102.
[4] T.Y. Tsang, R.L. Baldwin, E.L. Elson, Proc. Natl. Acad. Sci. U. S. A. 68 (1971) 2712–2715.
[5] H. Frauenfelder, S.G. Sligar, P.G. Wolynes, Science 254 (1991) 1598–1603.
[6] K.A. Dill, H.S. Chan, Nat. Struct. Biol. 4 (1997) 10–19.
[7] M. Karplus, Fold. Des. 2 (1997) S69–S75.
[8] J.N. Onuchic, Z. Luthey-Schulten, P.G. Wolynes, Annu. Rev. Phys. Chem. 48 (1997) 545–600.
[9] B.C. Dian, A. Longarte, T.S. Zwier, Science 296 (2002) 2369–2373.
[10] J.G. Lyubovitsky, H.B. Gray, J.R. Winkler, J. Am. Chem. Soc. 124 (2002) 5481–5485.
[11] S.O. Andrade, M.R.E. Silva, Biochem. J. 64 (1956) 701–705.
[12] R.B. Merrifield, J. Am. Chem. Soc. 86 (1964) 304–305.
[13] T. Wyttenbach, G. von Helden, M.T. Bowers, J. Am. Chem. Soc. 118 (1996) 8355–8364.
[14] E.A. Mason, E.W. McDaniel, Transport Properties of Ions in Gases, Wiley, New York, 1988.
[15] D.E. Clemmer, M.F. Jarrold, J. Mass Spectrom. 32 (1997) 577–592.
[16] T. Wyttenbach, M.T. Bowers, Top. Curr. Chem. 225 (2003) 207–232.
[17] G.F. Verbeck, B.T. Ruotolo, H.A. Sawyer, K.J. Gillig, D.H. Russell, J. Biomol. Tech. 13 (2002) 56–61.
[18] T. Wyttenbach, N.A. Pierson, D.E. Clemmer, M.T. Bowers, Ann. Rev. Phys. Chem. 65 (2014) 175–196.
[19] Most commonly used molecular dynamics programs for these types of applications include: GROMACS (Groningen Machine for Chemical Simu-

lations); Accelrys Discovery Studio; AMBER (Assisted Model Building and Energy Refinement); CHARMm (Chemistry at HARvard Macromolecular Mechanics); and NAMD.
[20] E. Mack, J. Am. Chem. Soc. 47 (1925) 2468–2482.
[21] A.A. Shvartsburg, M.F. Jarrold, Chem. Phys. Lett. 261 (1996) 86–91.
[22] M.F. Mesleh, J.M. Hunter, A.A. Shvartsburg, G.C. Schatz, M.F. Jarrold, J. Phys. Chem. 100 (1996) 16082–16086.
[23] P.D. Schnier, W.D. Price, R.A. Jockusch, E.R. Williams, J. Am. Chem. Soc. 118 (1996) 7178–7189.
[24] M.K. Green, C.B. Lebrilla, Int. J. Mass Spectrom. Ion Process. 175 (1998) 15–26.
[25] M.A. Freitas, C.L. Hendrickson, M.R. Emmett, A.G. Marshall, J. Am. Soc. Mass Spectrom. 9 (1998) 1012–1019.
[26] T. Wyttenbach, M.T. Bowers, J. Am. Soc. Mass Spectrom. 10 (1999) 9–14.
[27] A.E. Counterman, S.J. Valentine, C.A. Srebalus, S.C. Henderson, C.S. Hoaglund, D. E. Clemmer, J. Am. Soc. Mass Spectrom. 9 (1998) 743–759.
[28] T.G. Schaaff, J.L. Stephenson, S.A. McLuckey, J. Am. Chem. Soc. 121 (1999) 8907–8919.
[29] C.F. Rodriguez, G. Orlova, Y. Guo, X. Li, C.-K. Siu, A.C. Hopkinson, K.W.M. Siu, J. Phys. Chem. B 110 (2006) 7528–7537.
[30] S.L. Koeniger, S.I. Merenbloom, S.J. Valentine, M.F. Jarrold, H. Udseth, R.D. Smith, D.E. Clemmer, Anal. Chem. 78 (2006) 4161–4174.
[31] S.L. Koeniger, S.I. Merenbloom, S. Sevugarajan, D.E. Clemmer, J. Am. Chem. Soc. 128 (2006) 11713–11719.
[32] S.L. Koeniger, D.E. Clemmer, J. Am. Soc. Mass Spectrom. 18 (2007) 322–331.
[33] B.C. Bohrer, N. Atlasevich, D.E. Clemmer, J. Phys. Chem. B 115 (2011) 4509–4515.
[34] N.A. Pierson, L. Chen, S.J. Valentine, D.H. Russell, D.E. Clemmer, J. Am. Chem. Soc. 133 (2011) 13810–13813.
[35] N.A. Pierson, L. Chen, D.H. Russell, D.E. Clemmer, J. Am. Chem. Soc. 135 (2013) 3186–3192.
[36] N.A. Pierson, S.J. Valentine, D.E. Clemmer, J. Phys. Chem. B 114 (2010) 7777–7783.
[37] G.E. Spangler, Anal. Chem. 65 (1993) 3010–3014.
[38] T. Wyttenbach, G. von Helden, J.J. Batka Jr., D. Carlat, M.T. Bowers, J. Am. Soc. Mass Spectrom. 8 (1997) 275–282.
[39] J.A. McLean, B.T. Ruotolo, K.J. Gillig, D.H. Russell, Int. J. Mass Spectrom. 240 (2005) 301–315.
[40] H.A. Sawyer, J.T. Marini, E.G. Stone, B.T. Ruotolo, K.J. Gillig, D.H. Russell, J. Am. Soc. Mass Spectrom. 16 (2005) 893–905.
[41] B.C. Bohrer, S.I. Merenbloom, S.L. Koeniger, A.E. Hilderbrand, D.E. Clemmer, Annu. Rev. Anal. Chem. 1 (2008) 293–327.
[42] C.S. Hoaglund-Hyzer, A.E. Counterman, D.E. Clemmer, Chem. Rev. 99 (1999) 3037–3079.
[43] C.S. Hoaglund-Hyzer, J. Li, D.E. Clemmer, Anal. Chem. 72 (2000) 2737–2740.
[44] K. Tang, A.A. Shvartsburg, H.N. Lee, D.C. Prior, M.A. Buschbach, F.M. Li, A.V. Tolmachev, G.A. Anderson, R.D. Smith, Anal. Chem. 77 (2005) 3330–3339.
[45] L.S. Fenn, J.A. Mclean, Anal. Bioanal. Chem. 391 (2008) 905–909.
[46] S.J. Valentine, R.T. Kurulugama, B.C. Bohrer, S.I. Merenbloom, R.A. Sowell, Y. Mechref, D.E. Clemmer, Int. J. Mass Spectrom. 283 (2009) 149–160.
[47] S.A. Shaffer, K.Q. Tang, G.A. Anderson, D.C. Prior, H.R. Udseth, R.D. Smith, Rapid Commun. Mass Spectrom. 11 (1997) 1813–1817.
[48] S.A. Shaffer, D.C. Prior, G.A. Anderson, H.R. Udseth, R.D. Smith, Anal. Chem. 70 (1998) 4111–4119.
[49] C.S. Hoaglund, S.J. Valentine, C.R. Sporleder, J.P. Reilly, D.E. Clemmer, Anal. Chem. 70 (1998) 2236–2242.
[50] MOBCAL is available free of charge at http://www.indiana.edu/nano/software.html.
[51] C.J. Cassady, J. Wronka, G.H. Kruppa, F.H. Laukien, Rapid Commun. Mass Spectrom. 8 (1994) 394–400.
[52] M.T. Rodgers, P.B. Armentrout, Acc. Chem. Res. 37 (2004) 989–998.
[53] A. Mookherjee, P.B. Armentrout (2014), doi:10.1016/j.ijms.2014.06.012.
[54] D.J. Butcher, K.G. Asano, D.E. Goeringer, S.A. McLuckey, J. Phys. Chem. A 103 (1999) 8664–8671.
[55] K.M. Ervin, Chem. Rev. 101 (2001) 391–444.
[56] P.B. Armentrout, K.M. Ervin, M.T. Rodgers, J. Phys. Chem. A 112 (2008) 10071–10085.
[57] R.M. Moision, P.B. Armentrout, J. Phys. Chem. A 110 (2006) 3933–3946.
[58] P.B. Armentrout, A. Gabriel, R.M. Moision, Int. J. Mass Spectrom. 283 (2009) 56–68.
[59] A.L. Heaton, R.M. Moision, P.B. Armentrout, J. Phys. Chem. A 112 (2008) 3319–3327.
[60] J. Sztáray, A. Memboeuf, L. Drahos, K. Vékey, Mass Spectrom. Rev. 30 (2011) 298–320.
[61] R.C. Dunbar, Int. J. Mass Spectrom. Ion Process. 160 (1997) 1–16.
[62] J. Laskin, Energy and entropy effects in gas-phase dissociation of peptides and proteins, in: J. Laskin, J. Laskin, C. Lifshitz, C. Lifshitz (Eds.), Principles of Mass Spectrometry Applied to Biomolecules, John Wiley & Sons, Hoboken, NJ, 2006, pp. 619–665.
[63] T. Baer, P.M. Mayer, J. Am. Soc. Mass Spectrom. 8 (1997) 103–115.
[64] L. Sleno, D. Volmer, J. Mass Spectrom. 39 (2004) 1091–1112.
[65] K. Vékey, J. Mass Spectrom. 31 (1996) 445–463.
[66] J. Laskin, J.H. Futrell, Mass Spectrom. Rev. 22 (2003) 158–181.
[67] J. Laskin, J.H. Futrell, Mass Spectrom. Rev. 24 (2005) 135–167.
[68] A. Memboeuf, A. Nasioudis, S. Indelicato, F. Pollreisz, A. Kuki, S. Kéki, O.F. van den Brink, K. Vékey, L. Drahos, Anal. Chem. 82 (2010) 2294–2302.
[69] S. Indelicato, D. Bongiorno, S. Indelicato, L. Drahos, V.T. Liveri, L. Turiák, K. Vékey, L. Ceraulo, J. Mass Spectrom. 48 (2013) 379–383.
[70] Weighted linear regression takes into account uncorrelated errors in both the *x* and *y* dimensions. Analysis was performed in MATLAB (The MathWorks, Inc., Natick, Massachusetts, U.S.A.) with code from Thirumalai K., Singh A., Ramesh R., J. Geol. Soc. India 77 (2011) 377–380.
[71] M. Busman, A.L. Rockwood, R.D. Smith, J. Phys. Chem. 96 (1992) 2397–2400.
[72] R.C. Dunbar, T.B. McMahon, Science 279 (1998) 194–197.
[73] P.B. Armentrout, J. Mass Spectrom. 34 (1999) 74–78.
[74] R.G. Cooks, J.T. Koskinen, P.D. Thomas, J. Mass Spectrom. 34 (1999) 85–92.
[75] S. Bourgoin-Voillard, C. Afonso, D. Lesage, E.-L. Zins, J.-C. Tabet, P.B. Armentrout, J. Am. Soc. Mass Spectrom. 24 (2013) 365–380.
[76] S.-W. Lee, P. Freivogel, T. Schindler, J.L. Beauchamp, J. Am. Chem. Soc. 120 (1998) 11758–11765.
[77] J.A. Silveira, K.L. Fort, D. Kim, K.A. Servage, N.A. Pierson, D.E. Clemmer, D.H. Russell, J. Am. Chem. Soc. 135 (2013) 19147–19153.
[78] B. Paizs, S. Suhai, Mass Spectrom. Rev. 24 (2005) 508–548.
[79] V.H. Wysocki, G. Cheng, Q. Zhang, K.A. Herrmann, R.L. Beardsley, A.E. Hilderbrand, Peptide fragmentation overview, in: J. Laskin, J. Laskin, C. Lifshitz, C. Lifshitz (Eds.), Principles of Mass Spectrometry Applied to Biomolecules, John Wiley & Sons, Hoboken, NJ, 2006, pp. 279–300.
[80] M.J. Polce, D. Ren, C. Wesdemiotis, J. Mass Spectrom. 35 (2000) 1391–1398.
[81] N.C. Polfer, B.C. Bohrer, M.P. Plasencia, B. Paizs, D.E. Clemmer, J. Phys. Chem. A 112 (2008) 1286–1293.
[82] A.G. Harrison, Mass Spectrom. Rev. 28 (2009) 640–654.
[83] P.B. Armentrout, A.A. Clark, Int. J. Mass Spectrom. 182–191 (2012) 316–318.
[84] M. Moradi, V. Babin, C. Roland, T.A. Darden, C. Sagui, Proc. Natl. Acad. Sci. U. S. A. 106 (2009) 20746–20751.
[85] A.E. Tonelli, J. Am. Chem. Soc. 95 (1973) 5946–5948.
[86] C.M. Venkatachalam, B.J. Price, S. Krimm, Biopolymers 14 (1975) 1121–1132.
[87] Y.K. Kang, H.Y. Choi, Biophys. Chem. 111 (2004) 135–142.
[88] H.N. Cheng, F.A. Bovey, Biopolymers 16 (1977) 1465–1472.

Please cite this article in press as: N.A. Pierson, D.E. Clemmer, An IMS–IMS threshold method for semi-quantitative determination of activation barriers: Interconversion of proline *cis*↔*trans* forms in triply protonated bradykinin, Int. J. Mass Spectrom. (2014), http://dx.doi.org/10.1016/j.ijms.2014.07.012